# Supporting Information

## A Visible Light/Heat Responsive Covalent Organic Framework for Highly Efficient and Switchable Proton Conductivity

Yongkui Chen,[ab] Jikuan Qiu,[a] Xia-Guang Zhang,[a] Huiyong Wang,[a] Wenhui Yao,[b] Zhiyong Li,[a] Qingchun Xia,[a] Guangshan Zhu*[c] and Jianji Wang*[a]

[a]*Collaborative Innovation Center of Henan Province for Green Manufacturing of Fine Chemicals, School of Chemistry and Chemical Engineering, Key Laboratory of Green Chemical Media and Reactions, Ministry of Education, Henan Normal University, Xinxiang, Henan 453007, P. R. China.*

[b]*School of Chemistry and Materials Engineering, Xinxiang University, Xinxiang, Henan, 453003, P. R. China.*

[c]*Key Laboratory of Polyoxometalate and Reticular Material Chemistry of Ministry of Education, Faculty of Chemistry, Northeast Normal University, Changchun 130024, P. R. China.*

**Table of Contents**

## 1. Materials and Instrumentation methods

**Materials:** 1,3,5-triformylphloroglucinol (Tp, 98%, Macklin), methyl 4-aminosalicylate (97%, J&K Scientific, Ltd.), hydrazinium hydrate (80%, Aladdin), ethanol (99.5%, J&K Scientific, Ltd.), 2-furaldehyde (99%, Alfa Aesar), meldrum's acid (98%, Alfa Aesar), cyclohexane (99%, Aladdin), ethyl acetate (99.5%, Aladdin), dioxane (99%, Sigma-Aldrich), mesitylene (98%, Sigma-Aldrich), acetic acid (99.9%, J&K Scientific, Ltd.), triethylamine (99%, Macklin), glycidol (Glc, 97%, Macklin ), and (3-butylaminopropyl) trimethoxysilane (BAPTMS, 98%, TCI) were used in the present work. All starting materials and solvents, unless otherwise specified, were used without further purification. Deionized water was used in this study.

**Instrumentation Methods:** FT-IR spectrum was collected on a Spectrum 400 spectrometer (Perkin-Elmer). Powder X-ray diffraction (PXRD) patterns were recorded on a Bruker D8 Advance diffractometer from $2\theta = 2°$ to $40°$ in $0.1°$ increment at 40 kV and 20 mA. The thermal properties of the materials were evaluated using a thermogravimetric analysis (TGA) instrument (STA449C) over the temperature range from 25 to 800 ºC at a heating rate of 10 ºC $min^{-1}$ under $N_2$ atmosphere. The Brunauer-Emmett-Teller (BET) specific surface area measurements were performed on a Quantachrome instrument (ASIQM 00002200-7 system). Field-emission scanning electron microscope (FE-SEM) observations were performed to obtain images of COFs films on a Hitachi SU8010 microscope at an accelerating voltage of 10.0 kV. TEM images were obtained on a JEM-2010 transmission electron microscope operated at an accelerating voltage of 200 kV. X-ray photoelectron spectra (XPS) were collected with an ESCALab220Xi Thermo Scientific electron spectrometer. $^{1}H$ NMR spectra were recorded on a Bruker AVANCE III HD 600 spectrometer where deuterated solvents (DMSO-d6) were used. $^{13}C$ CP MAS Solid-state NMR experiments were conducted on an Agilent 600 MHz spectrometer. Water contact angles were measured on a DSA25 KRUSS

drop shape analyzer. The water vapor uptake and release experiments were carried out using an ASAP 2460 adsorption instrument.

**2. Synthetic Procedures**

**Synthesis of 5-(Furan-2-ylmethylene)-2,2-dimethyl-1,3-dioxane-4,6-dione**

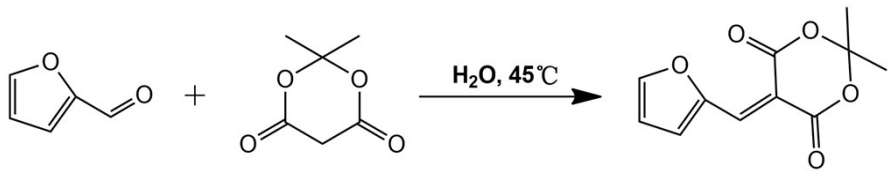


**Scheme S1.** Synthesis of the building unit of the donor-acceptor Stenhouse adducts.

5-(Furan-2-ylmethylene)-2,2-dimethyl-1,3-dioxane-4,6-dione is the building unit of donor-acceptor Stenhouse adducts (DASAs), which was synthesized according to the procedures reported in literature[1] with slight modification. To this end, Meldrum's acid (1.51 g, 10.5 mmol) and 2-furaldehyde (0.83 mL, 10 mmol) were mixed with water (30 mL) under $N_2$ atmosphere at 25 ℃. Then the mixture was reacted at 60 ℃ for 2h. After completion of the reaction (monitored by TLC, hexane : ethyl acetate = 3:1), the mixture was cooled to room temperature. The precipitate was collected by vacuum filtration and washed twice with 30 mL of water. The resulted solid was dissolved in dichloromethane, washed sequentially with aqueous saturated $NaHSO_3$, water, aqueous saturated $NaHCO_3$ and brine. The organic layer was dried over $MgSO_4$ and the solvent was removed by rotary evaporation to give 2.10 g (95%) of the product as a bright yellow powder. $^1$H NMR (600 MHz, $CDCl_3$): δ = 8.47 (d, 1H, *CH*), 8.36 (s, 1H, *CH*), 7.85 (d, 1H, *CH*), 6.76 (ddd, 1H, *CH*), 1.77 (s, 6H; *2CH$_3$*) ppm.

**Synthesis of the small molecule DASA**

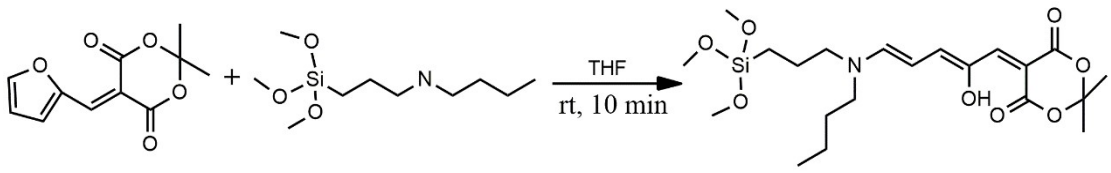


**Scheme S2.** Synthesis of the small molecule DASA from (3-butylaminopropyl) trimethoxysilane and activated furans.

The small molecule DASA was synthesized from (3-butylaminopropyl) trimethoxysilane and activated furans according to the procedures reported in literature.[1] Typically, the activated furans of 5-(furan-2-ylmethylene)-2,2-dimethyl -1,3-dioxane-4,6-dione (0.6 gram, 2.7 mmol) was dissolved in 10 ml of tetrahydrofuran. Then, (3-butylaminopropyl) trimethoxysilane (0.67 ml, 2.7 mmol) was added to this solution. After being stirred for 10 min at room temperature, the solution was cooled to 0 ℃ in ice water and further stirred for 20 min, and then filtered to collect the precipitated solid. This solid was washed with cold diethyl ether three times, and dried under vacuum to afford the small DASA molecules as a purple solid.

$^{1}$H NMR (600 MHz, $CDCl_3$): δ 11.42 (s, 1H, *OH*), 7.21 (d, 1H, *CH*), 7.08 (s, 1H, *CH*), 6.71 (dd, 1H, *CH*), 6.04 (t, 1H, *CH*), 3.40 (m, 6H, $CH_2$), 3.02 (s, 9H, $CH_3$), 1.72 (s, 6H, $CH_3$), 1.67 (m, 4H, $CH_2$), 1.39 (m, 2H, $CH_2$), 0.96 (t, 3H, $CH_3$) ppm.

$^{13}$C NMR ($CDCl_3$): δ 167.09, 165.40, 156.51, 150.91, 144.96, 139.64, 103.49, 101.99, 90.81, 51.85, 44.05, 26.71, 14.55, 12.29 ppm.

**Synthesis of 4-aminosalicylhydrazide (ASH)**

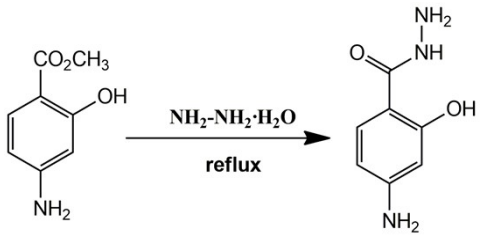


**Scheme S3.** Synthesis of 4-aminosalicylhydrazide.

ASH was prepared according to the procedures described in the literature.[2,3] Here, 2.0 g of methyl-4-aminosalicylate was added to about 8 mL of 80% hydrazine monohydrate. The resultant mixture was refluxed for 90 min under nitrogen atmosphere. After evaporation of excess hydrazine monohydrate, 15 mL of ice-cold distilled water was added in the product. Then the system was filtrated under vacuum, and crude ASH was collected and recrystallized from 100 ml distilled water to produce purified ASH (Yield: 1.0g, 50%).

**Synthesis of TpASH. TpASH** was synthesized using solvothermal approach. In a typical experiment, 1,3,5-triformylphloroglucinol (Tp, 0.12 mmol, 18.0 mg) and 4-aminosalicylhydrazide (ASH, 0.08 mmol, 28.1 mg) were put into a 10 mL Pyrex tube, then a solution of dioxane / mesitylene / 6 M acetic acid (1 mL/1 mL/0.2 mL) was added. This mixture was sonicated for 10 min to get a homogenous dispersion. The tube was then flash-frozen at 77K and degassed by three freeze-pump-thaw cycles. The tube was sealed off and then kept in an oven without stirring at 120°C for 3 days. After being cooled to room temperature, the obtained solid was collected and washed with dimethyl formamide, water, and ethanol for three times, respectively. The precipitate was dried at 120 °C under vacuum for 12 h to obtain the corresponding yellow colored product. Elemental analysis (N, C, and H) of **TpASH** was recorded on a Thermo Scientific elemental analyzer (Model: Elementar UNICUBE). The experimental values (C, 51.89%; H, 4.88%; N, 13.27%) were close to those (C, 57.56%; H, 3.32%; N, 15.50%) estimated from an infinite 2D sheet ($C_{13}H_9N_3O_4$).

**3. Nyquist plots under ideal conditions**

Conventionally, under ideal conditions, Nyquist plot is composed of a semicircular arc at the high-frequency region and a straight line with a $45^o$ slope at the low frequency region as shown in Scheme S4. In this plot, the distance from the origin to A at which the beginning of the arc intersects the Z'-axis corresponds to the value of ohmic resistance (internal resistance). The diameter of the semicircle (distance from A to C) corresponds to the value of charge-transfer resistance, and the distance from the origin to B where the extension of the straight line intersects the Z'-axis is related to the value of charge-diffusion resistance.[4]

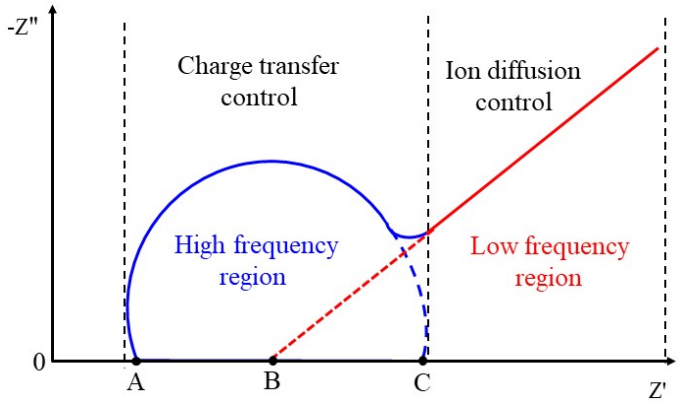


**Scheme S4.** Nyquist plots under ideal conditions.

**4. Evaluation of proton transport number**

The proton transport number was evaluated in the temperature range from 25 to 80 ℃ from alternating current conductivity under wet and dry conditions assuming proton conduction has no effect on other charge carriers' contribution. Under this condition, the proton transport number was calculated by using the following equation:[5]

$$t_H = \frac{\sigma_{wet} - \sigma_{dry}}{\sigma_{wet}} \qquad (1)$$

where $t_H$ is the proton transport number, $\sigma_{wet}$ and $\sigma_{dry}$ are the bulk conductivity with and without water vapor at a given temperature, respectively.

**5. DFT calculations**

The calculations were performed by Gaussian 16 program.[6] The hybrid exchange-correlation functional B3LYP was employed to optimize all structures of the ground states. The 6-311+G (d, p) was adopted for the basis set of H, C, N and O atoms. The tight option of the cutoffs on forces and step size was used to determine convergence. Vibrational frequency calculations showed that all optimized structures were minima on the potential energy surfaces of the electronic ground states. Furthermore, in order to illustrate the charge transport and reduce the computational expense, a dimer structure fragment was built to describe the **COF-HNU9** framework. To better illustrate the abundant hydrogen-bond networks existed in the framework of **COF-HNU9**, many water molecules were used to describe the process and

connect the two DASA groups on the dimer structure fragment in building the models with water for our DFT calculation. The criteria of choosing the number of water molecules was that it satisfied with the local hydrogen-bond network, while **COF-HNU9** framework was not affected. The calculated energy for HOMO of non-water and water environment was -5.62 and -5.32 eV, and that for corresponding LUMO was -3.04 and -3.57 eV, respectively.

**6. Switchable lighting and turning off of a light-emitting diode (LED) lamp**

First, the as-prepared **COF-HNU9** sample was mechanically pressed into rounded films with a thickness from 0.5 to 2 mm. Then, the film was sandwiched in two stainless steel sheets which were then connected to the circuit with a long copper wire. The film was placed in a constant temperature and humidity chamber at 80 ℃ and 98% RH. After the film was irradiated by visible light, **COF-HNU9** existed mainly in its closed and hydrophilic form of **COF-HNU9-C**, and its conductivity increased enough to light up the LED lamp. Then the film was heated at 40 ℃ in the dark under 32% RH. On this occasion, the open and hydrophobic **COF-HNU9-O** was the main existing form, and the proton conductivity was greatly reduced, and the LED lamp was switched off.

**7. Fig. S1-S21**

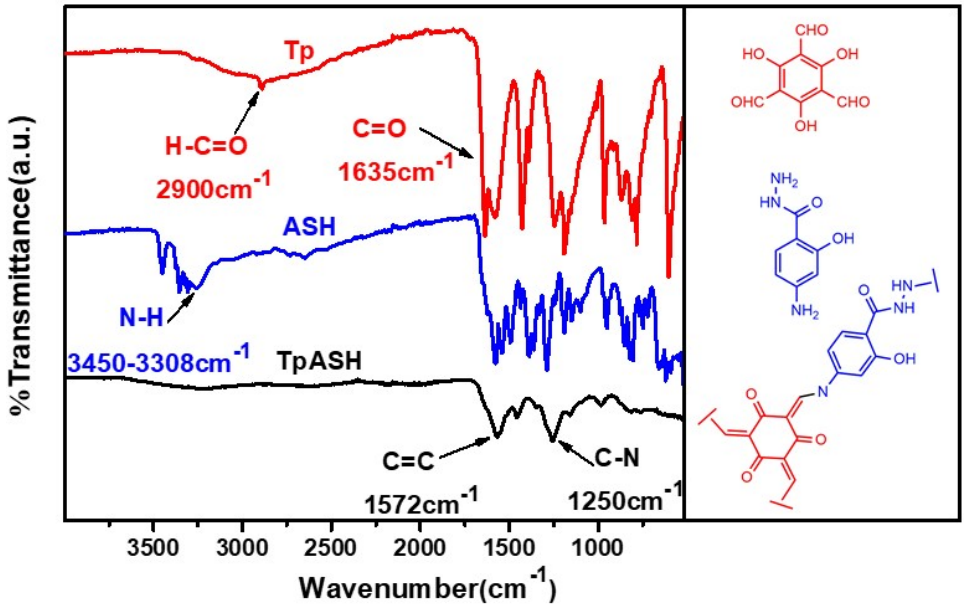


**Fig. S1** Comparison of FTIR spectra among Tp, ASH and **TpASH**.

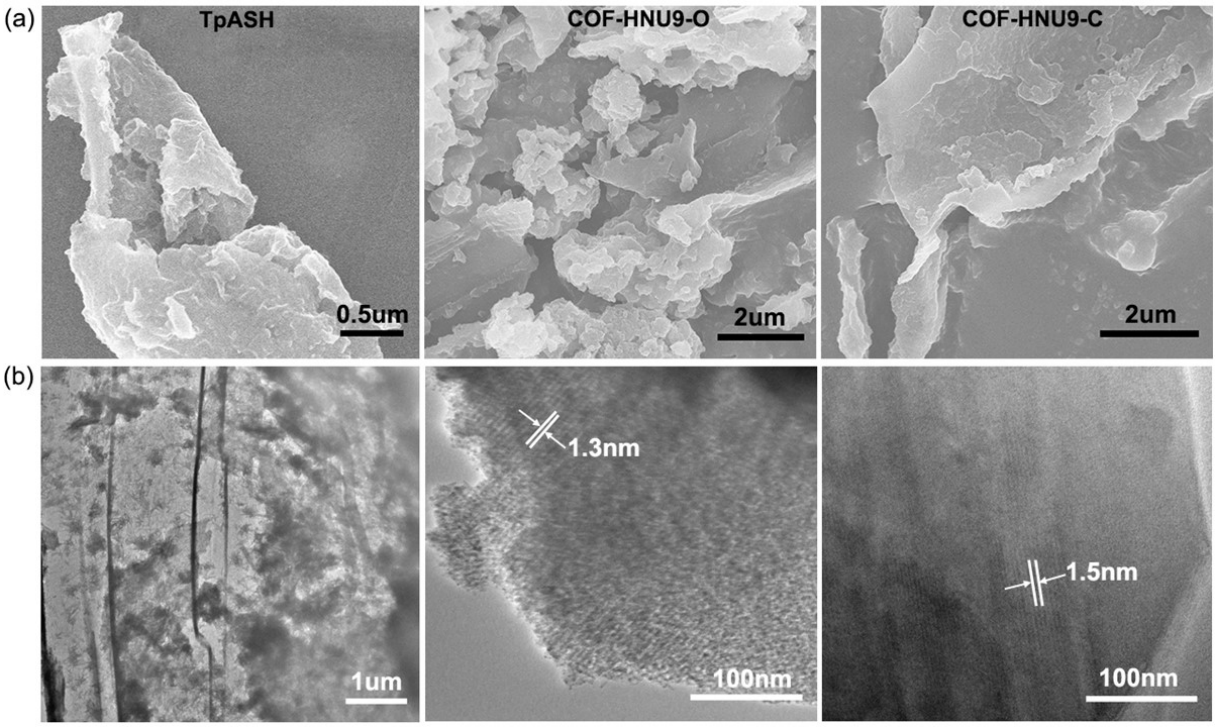


**Fig. S2** SEM (a) and TEM images (b) of the as-synthesized **TpASH** and **COF-HNU9** before and after visible light irradiation.

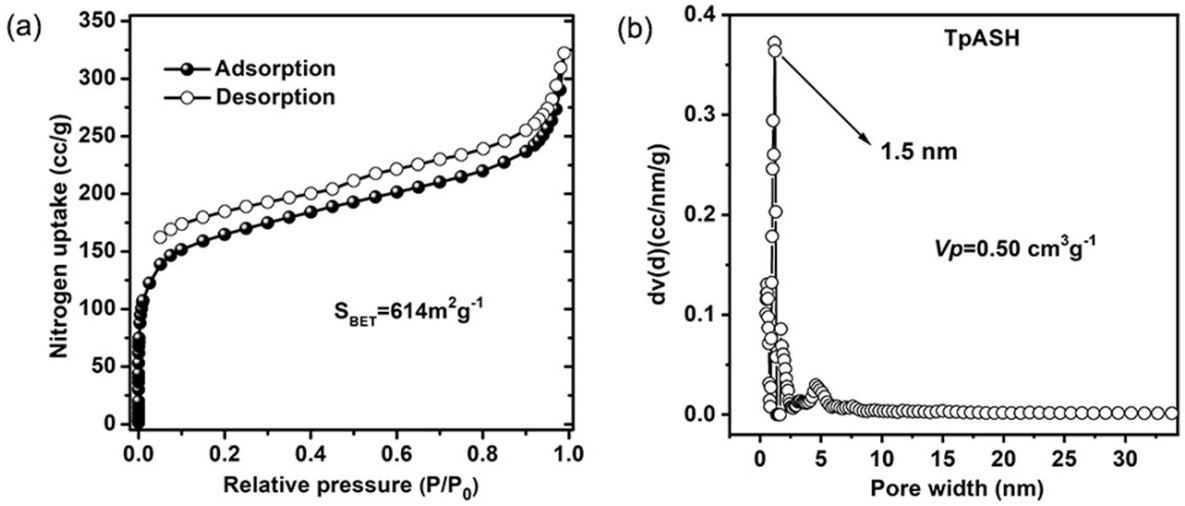


**Fig. S3** $N_2$ sorption isotherms (a) and DFT pore size distribution (b) of **TpASH** by using nonlocal density functional theory (NLDFT). The total pore volume of **TpASH** was estimated to be 0.50 $cm^3g^{-1}$.

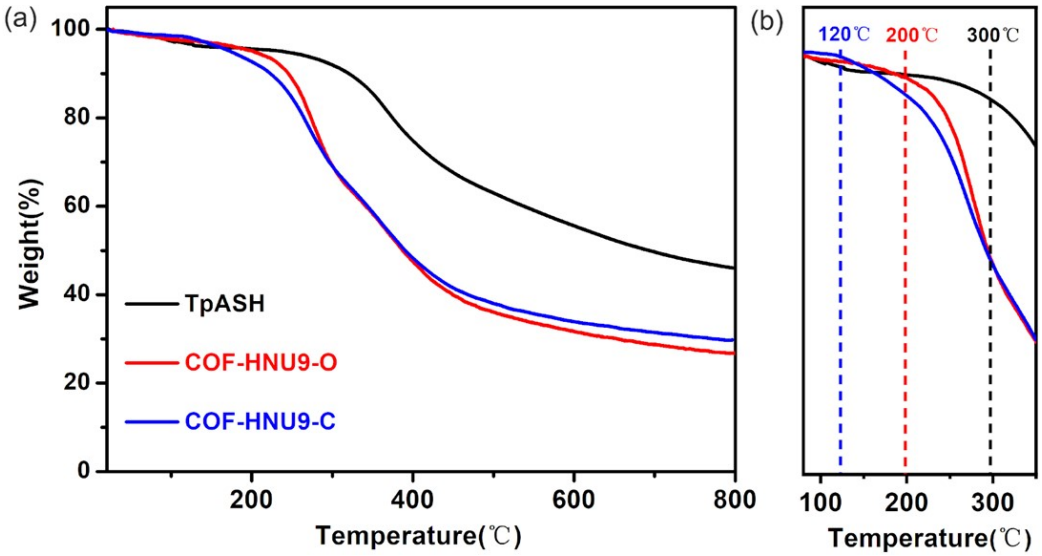


**Fig. S4** TGA profiles (a) and the enlarged view between 80 and 350 ℃ (b) of **TpASH** (dark curve) and **COF-HNU9** before (red curve) and after (blue curve) visible light irradiation, indicating that the thermal decomposition temperature of **TpASH**, **COF-HNU9-O** and **COF-HNU9-C** are 300, 200 and 120 °C, respectively.

Note: The loading values ($\mathbf{L_{mol}}$) of DASA on the **COF-HNU9**, expressed by mole percent, was calculated according to the following equation:

$$L_{mol} = \frac{(1 - R_{COF-HNU9}) - (1 - R_{TpASH})}{M_{DASA}} \qquad (2)$$

where $R_{COF\text{-}HNU9}$ and $R_{TpASH}$ are residual mass percent of **COF-HNU9** and **TpASH**, respectively, and $M_{DASA}$ is the molar mass of DASA appendant.

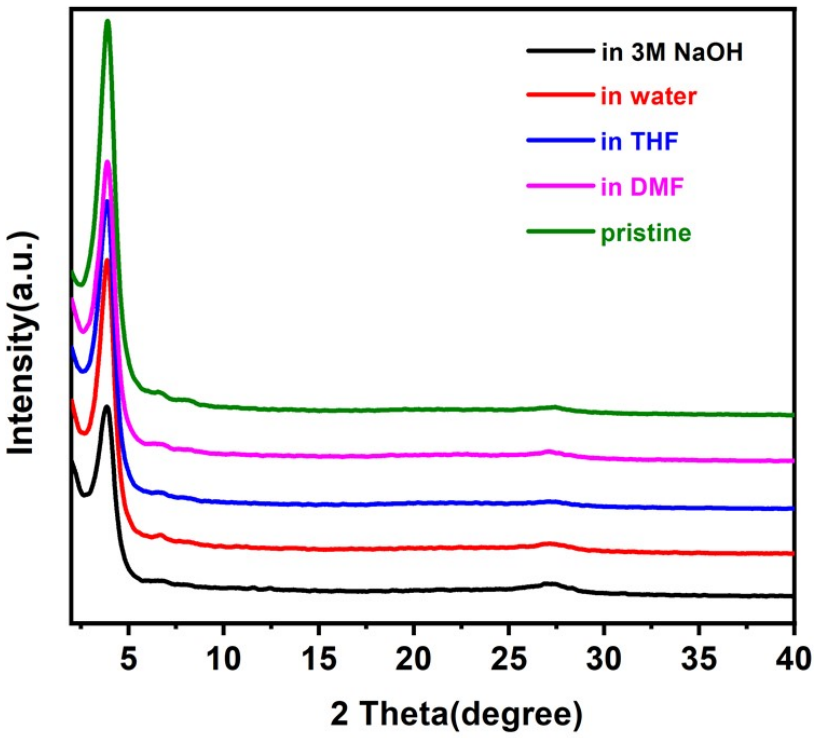


**Fig. S5** PXRD patterns of **TpASH** after treatment by different solvents.

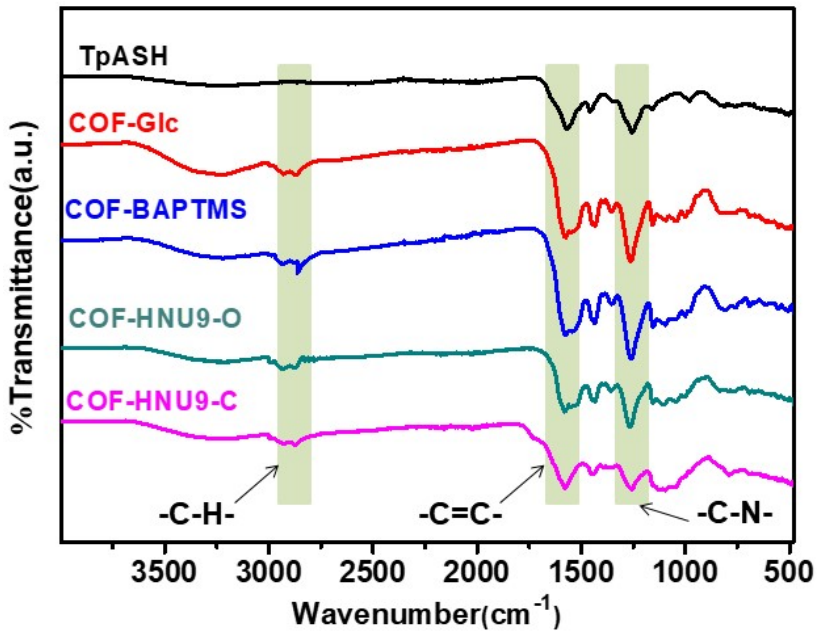


**Fig. S6** Comparison of FTIR spectrum of the as-prepared **COF-HNU9** with its precursors.

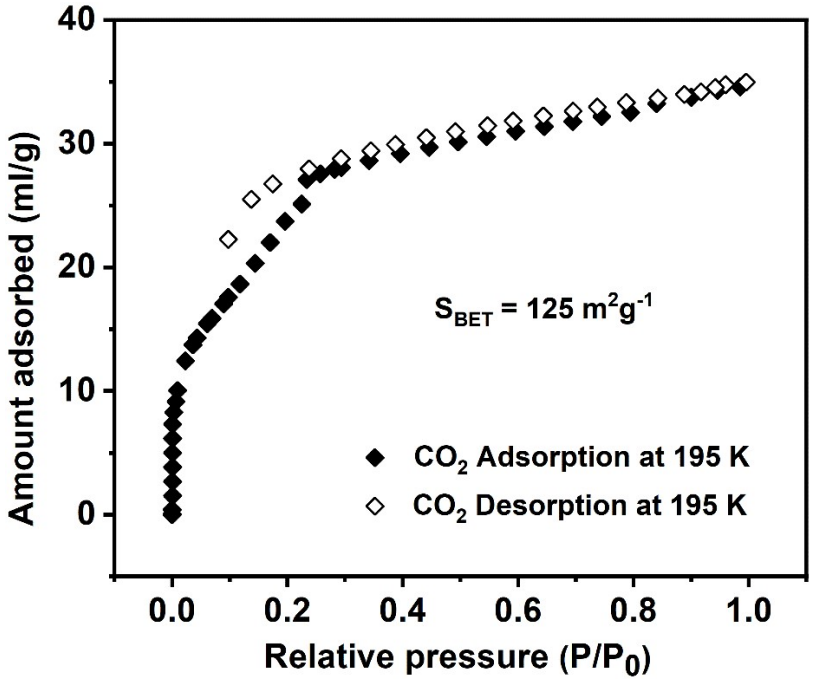


**Fig. S7** $CO_2$ adsorption (solid) and desorption (open) isotherms for **COF-HNU9** at 195 K.

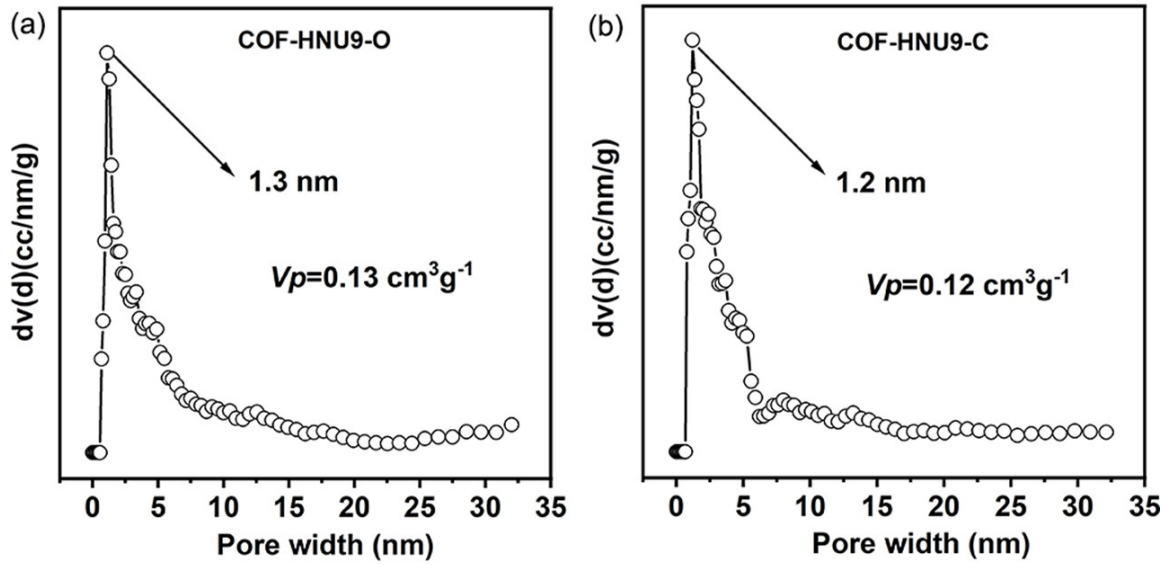


**Fig. S8** DFT pore size distribution of **COF-HNU9** before (a) and after (b) visible light irradiation by using nonlocal density functional theory (NLDFT). The total pore volume of **COF-HNU9-O** and **COF-HNU9-C** was estimated to be 0.13 and 0.12 $cm^3g^{-1}$, respectively.

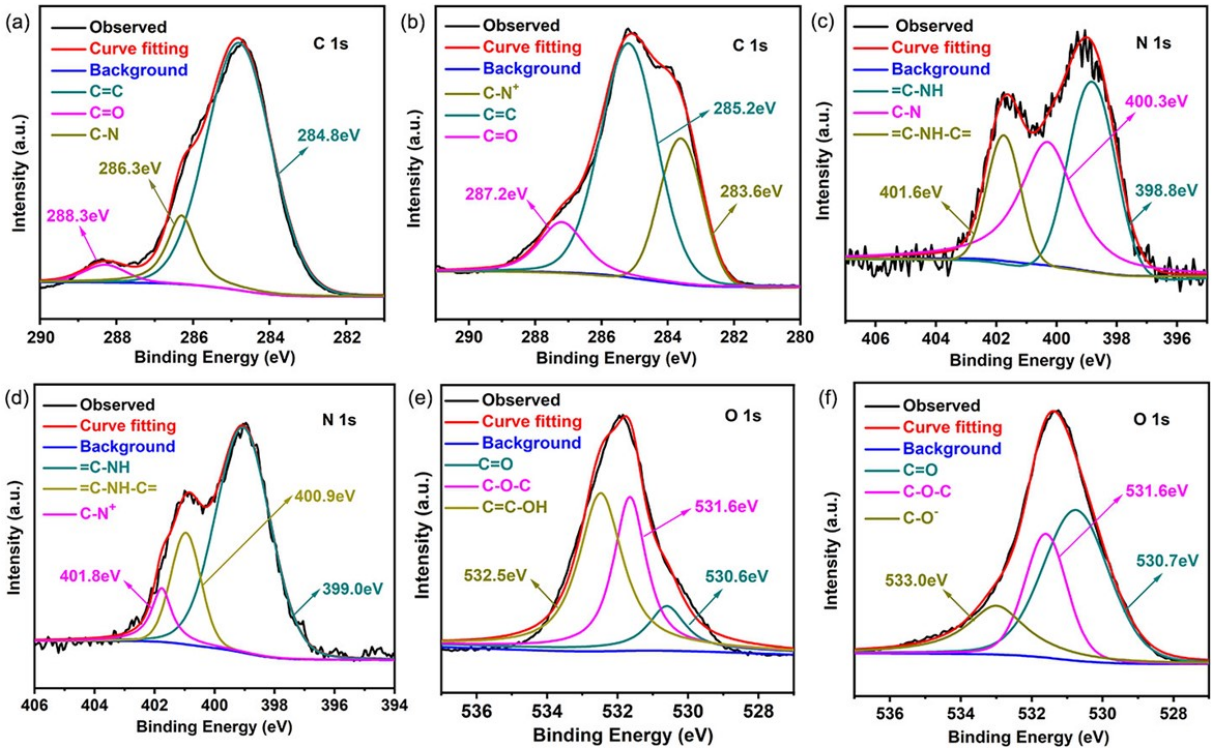


**Fig. S9** Curve fitting of C1s (a)-(b), N1s (c)-(d), and O1s signals (e, f) in XPS spectra of **COF-HNU9** before and after visible light irradiation.

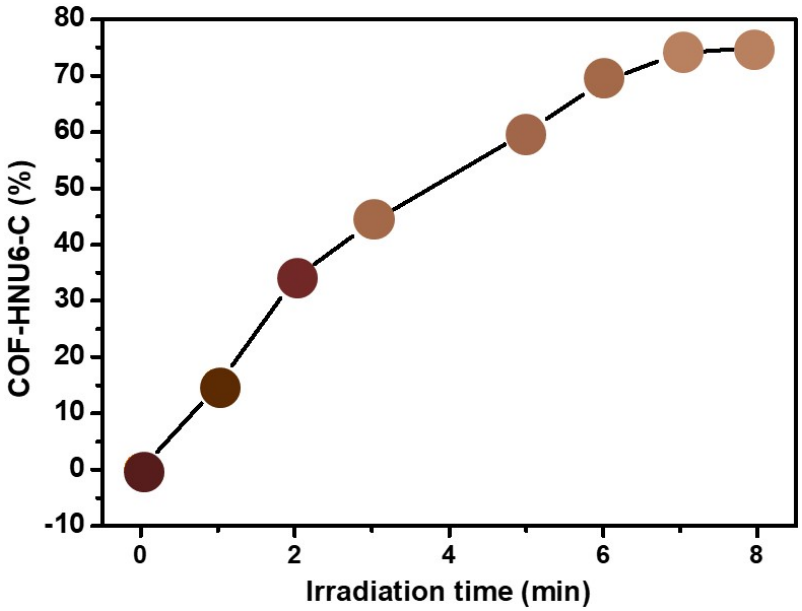


**Fig. S10** Fraction change of **COF-HNU9-C** isomer after visible light irradiation (at 515 nm) on **COF-HNU9-O**.

The percentage of **COF-HNU9-C** isomer was calculated from the following equation:

$\%_{close} = (A_{open} - A_{close}) * 100 / A_{open}$, where $A_{open}$ = maximum absorbance of **COF-HNU9-O**, and $A_{close}$ = maximum absorbance of **COF-HNU9-C**.

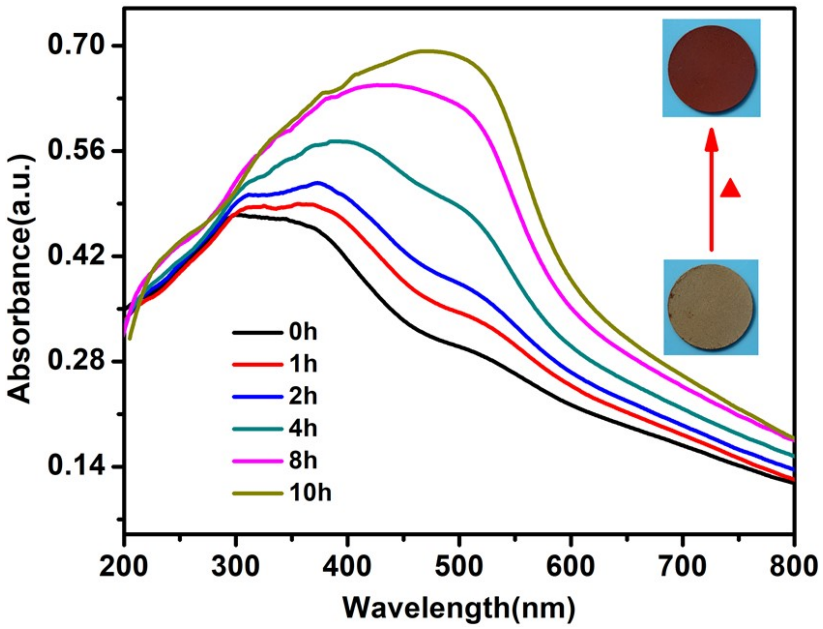


**Fig. S11** UV-vis spectra of **COF-HNU9-C** at 40 ℃ for different heating time.

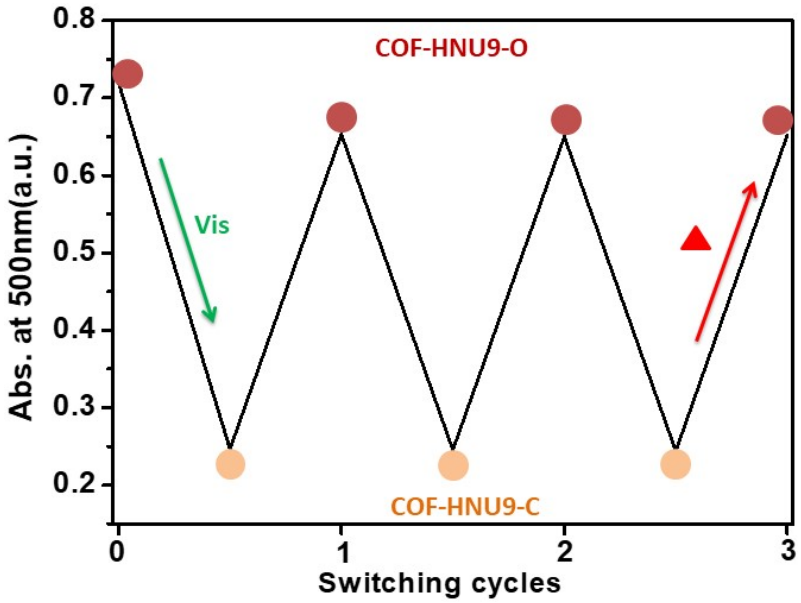


**Fig. S12** Three stimuli-switching cycles of **COF-HNU9** in solid state upon alternating irradiation of visible light and heating at 40 ℃.

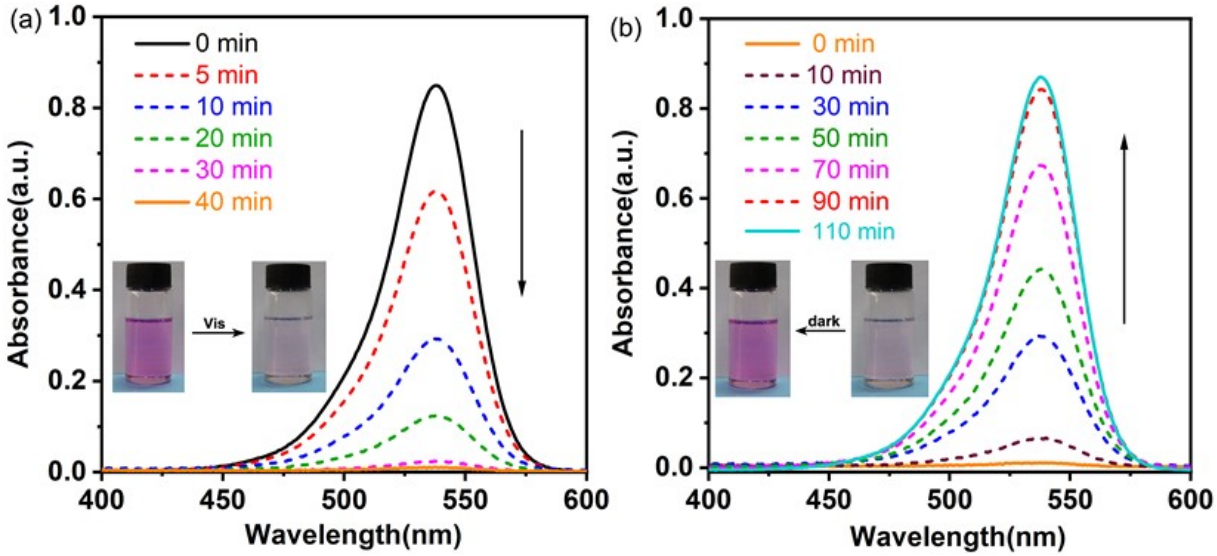


**Fig. S13** UV-visible absorption spectra of the small DASA molecules synthesized from (3-butylaminopropyl) trimethoxysilane and activated furans upon irradiation with visible light in ethyl acetate for 40 min (a), and followed by 110 min in the dark (b). Insert: photographs of the reversible isomerization of the DASA molecules in ethyl acetate.

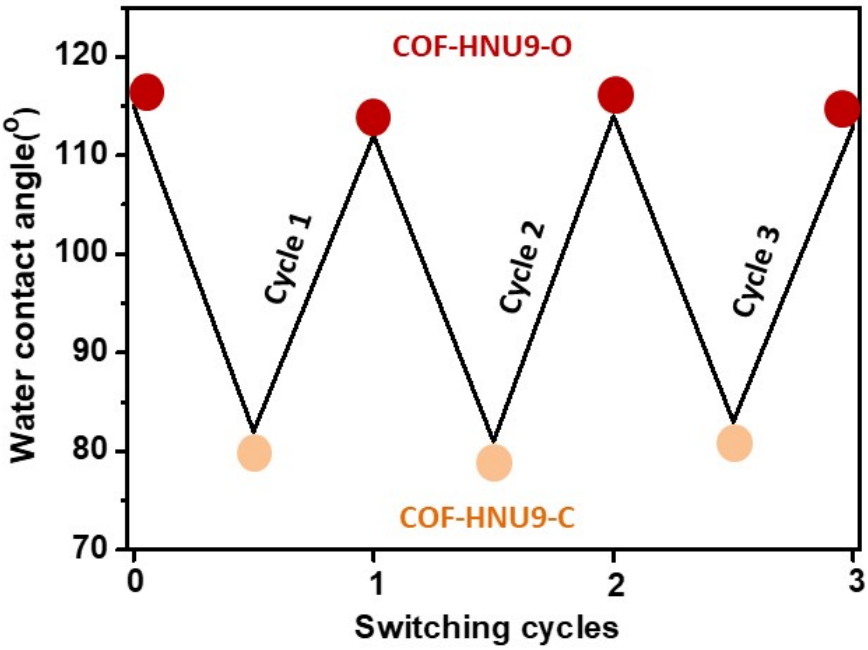


**Fig. S14** Three cycles showing the reversible wettability switching of **COF-HNU9** upon alternating irradiation with visible light for 8h followed by heating at 40 ℃ for 10 h.

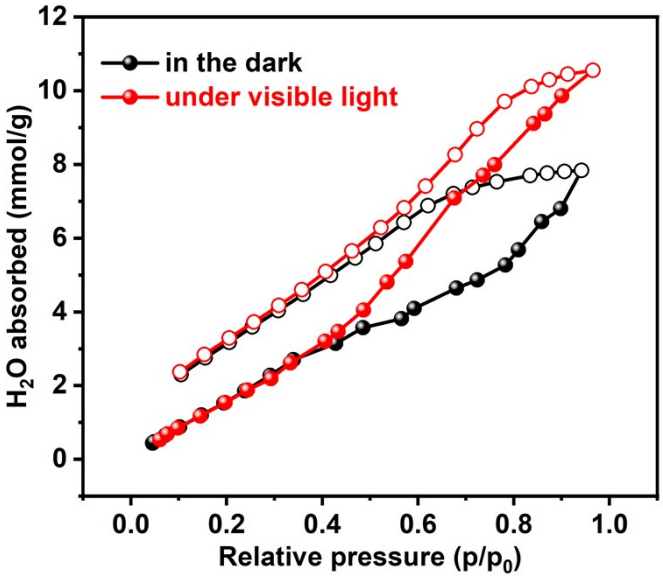


**Fig. S15** Water vapor sorption isotherms of **COF-HNU9** samples at 25 °C before and after irradiation with visible light (adsorption, filled; desorption, open).

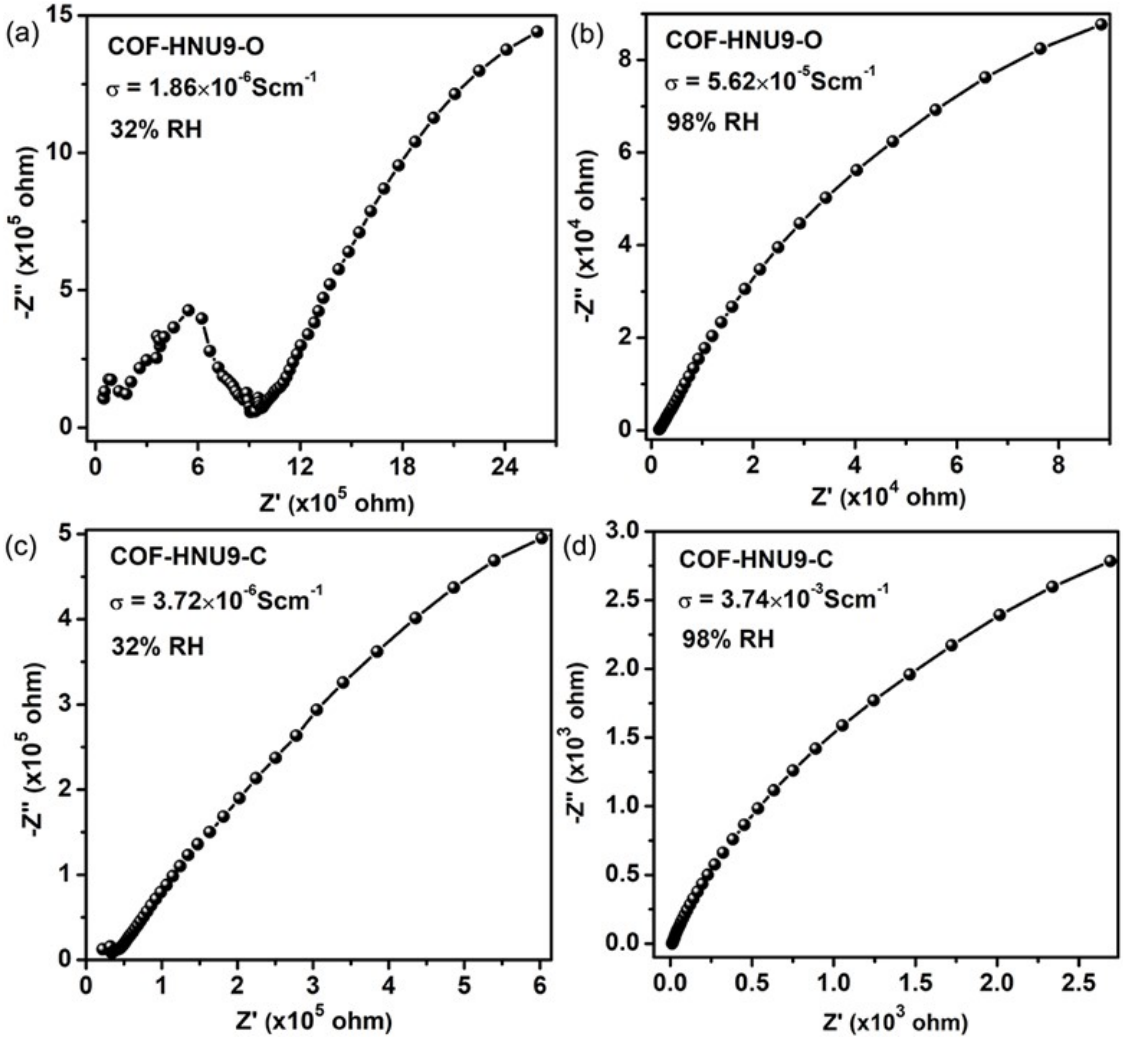


**Fig. S16** Nyquist plots of **COF-HNU9** samples measured under 32% and 98% RH at 25 °C before ((a)-(b)) and after ((c)-(d)) irradiation with visible light.

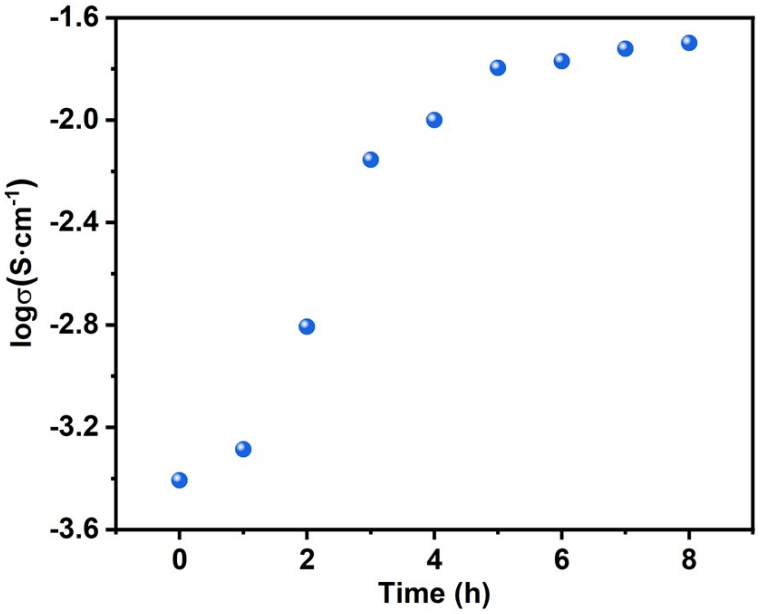


**Fig. S17** Time-dependent conductivity changes caused by the transformation of DASA units from neutral to zwitterionic state in **COF-HNU9** upon irradiation with visible light at 80 ℃.

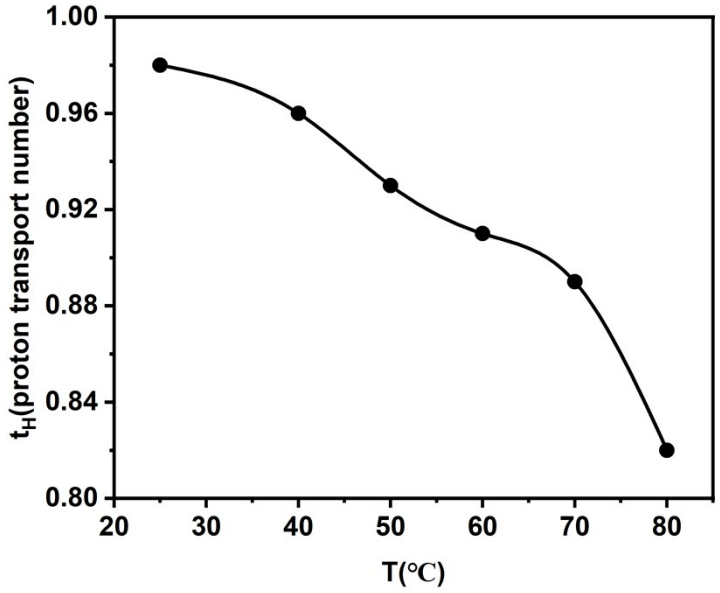


**Fig. S18** Proton transport number of **COF-HNU9** measured by alternating current conductivity with and without water vapor.

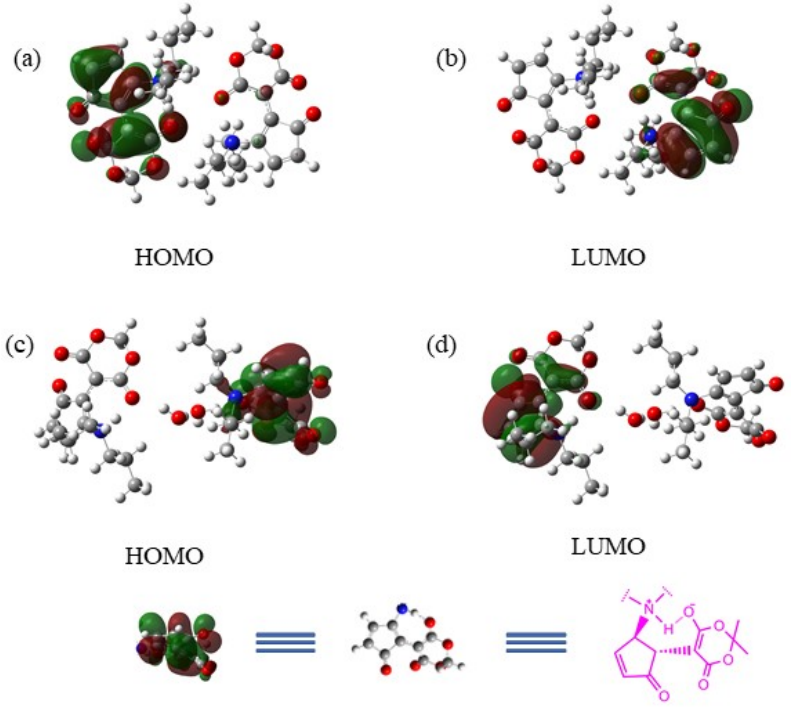


**Fig. S19** Frontier molecular orbitals of the small DASA groups without **COF-HNU9** framework in non-water (a, b) and water environments (c, d) (C, Gray; N, blue; O, red; H, white). All geometric structure optimizations were performed at the B3LYP/6-311+G (d, p) level. The calculated energy for HOMO in non-water and water environment was -5.80 and -5.75 eV, and that for corresponding LUMO was -3.11 and -3.26 eV, respectively.

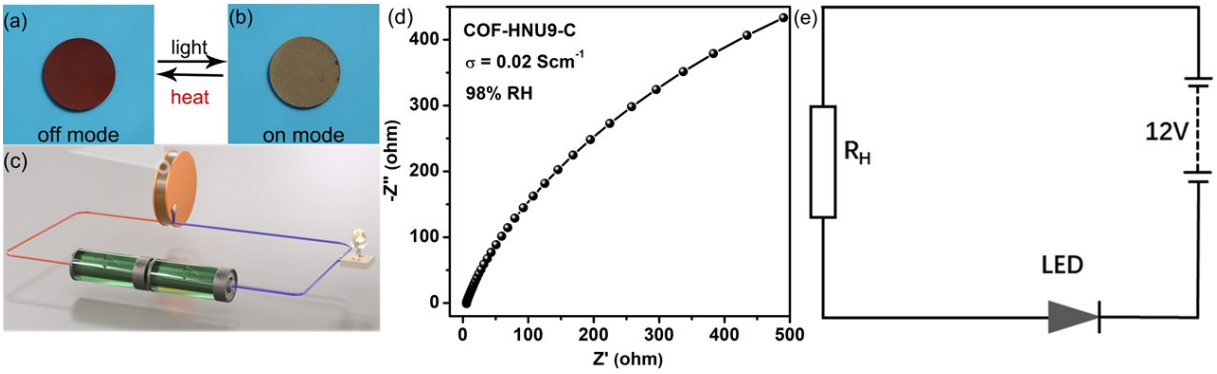


**Fig. S20** Illustrations of the **COF-HNU9** film before (a) and after (b) irradiation of visible light as well as the optically controlled circuit (c) to turn on/off the LED lamp without any amplifier. (d) Nyquist plots of **COF-HNU9** samples measured at 98% RH and 80 °C. (e) Equivalent circuit model representation for the proton conduction in **COF-HNU9**.

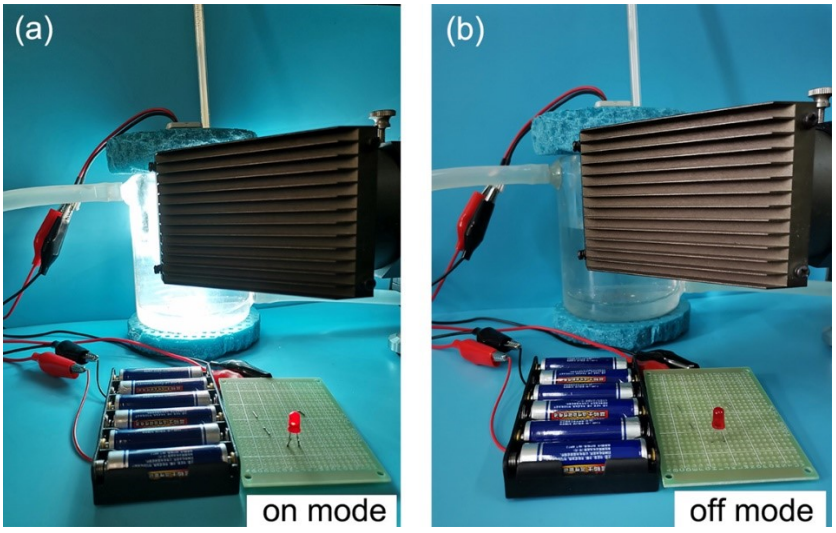


**Fig. S21** Photographs of the optical controlled circuit to light up the LED without any amplifier by turning on/off light illumination on the **COF-HNU9** film: (a) on mode (under visible light), (b) off mode (no visible light).

## 8. References

1 S. Helmy, F. A. Leibfarth, S. Oh, J. E. Poelma, C. J. Hawker and J. Read de Alaniz, *J. Am. Chem. Soc.*, 2014, **136**, 8169-8172.

2 H. Yamada, M. Kojo, T. Nakahara, K. Murakami, T. Kakima, H. Ichiba, T. Yajima and T. Fukushima, *Spectrochim. Acta Mol. Biomol. Spectrosc.*, 2012, **90**, 72-77.

3 S. Mitra, H. S. Sasmal, T. Kundu, S. Kandambeth, K. Illath, D. Díaz Díaz and R. Banerjee, *J. Am. Chem. Soc.*, 2017, **139**, 4513-4520.

4 H. Farahani, R. Wagiran and G. A. Urban, *IEEE Sens. J.*, 2021, **21**, 9657-9666.

5 G. Zhang and D.M. Smyth, *Solid State Ionics*, 1995, **82**, 153-156.

6 M. J. Frisch, G. W. Trucks, H. B. Schlegel, G. E. Scuseria, M. A. Robb, J. R. Cheeseman, G. Scalmani, V. Barone, G. A. Petersson, H. Nakatsuji, X. Li, M. Caricato, A. V. Marenich, J. Bloino, B. G. Janesko, R. Gomperts, B. Mennucci, H. P. Hratchian, J. V. Ortiz, A. F. Izmaylov, J. L. Sonnenberg, Williams, F. Ding, F. Lipparini, F. Egidi, J. Goings, B. Peng,

A. Petrone, T. Henderson, D. Ranasinghe, V. G. Zakrzewski, J. Gao, N. Rega, G. Zheng, W. Liang, M. Hada, M. Ehara, K. Toyota, R. Fukuda, J. Hasegawa, M. Ishida, T. Nakajima, Y. Honda, O. Kitao, H. Nakai, T. Vreven, K. Throssell, J. A. Montgomery Jr., J. E. Peralta, F. Ogliaro, M. J. Bearpark, J. J. Heyd, E. N. Brothers, K. N. Kudin, V. N. Staroverov, T. A. Keith, R. Kobayashi, J. Normand, K. Raghavachari, A. P. Rendell, J. C. Burant, S. S. Iyengar, J. Tomasi, M. Cossi, J. M. Millam, M. Klene, C. Adamo, R. Cammi, J. W. Ochterski, R. L. Martin, K. Morokuma, O. Farkas, J. B. Foresman and D. J. Fox, *Gaussian 16, Rev. C.01*, Wallingford, CT, **2016**.